Acta Crystallographica Section A
Foundations of Crystallography
ISSN 0108-7673

Received 25 April 2008
Accepted 29 September 2008

© 2009 International Union of Crystallography
Printed in Singapore – all rights reserved

Computation and parametrization of the temperature dependence of Debye–Waller factors for group IV, III–V and II–VI semiconductors

M. Schowalter,[a]* A. Rosenauer,[a] J. T. Titantah[b] and D. Lamoen[b]

[a]Institut für Festkörperphysik, Universität Bremen, D 28359 Bremen, Germany, and [b]Electron Microscopy for Materials Research (EMAT), Universiteit Antwerpen, B-2020 Antwerpen, Belgium. Correspondence e-mail: schowalter@ifp.uni-bremen.de

We calculated the temperature dependence of the Debye–Waller factors for a variety of group IV, III–V and II–VI semiconductors from 0.1 to 1000 K. The approach used to fit the temperature dependence is described and resulting fit parameters are tabulated for each material. The Debye–Waller factors are deduced from generalized phonon densities of states which were derived from first principles using the *WIEN2k* and the *ABINIT* codes.

1. Introduction

Quantitative transmission electron microscopy (TEM) relies on the comparison of experimental and simulated images. For dynamical image simulation a set of material parameters are required such as the Fourier components of Coulomb potentials and Debye–Waller factors. Fourier components are usually derived from atomic scattering amplitudes, which are typically taken from Doyle & Turner (1968) or Weickenmeier & Kohl (1991). Since atomic scattering amplitudes are computed for isolated atoms they do not take into account the redistribution of electrons due to bonds. However, accurate Fourier components can be derived using density functional theory (Zuo *et al.*, 1997; Rosenauer *et al.*, 2005). In addition to an accurate Coulomb potential one has to take into account the influence of the thermal vibration of the atoms. In this respect different schemes have been developed. The most common method uses damping factors of Bragg reflections that contain the Debye–Waller factor (see *e.g.* Kittel, 1988). Using a damping factor for the incorporation of the effect of the temperature on the Bragg reflections is accurate for X-ray scattering or neutron scattering, but may lead to significant errors in the simulation of electron scattering (Rother & Lichte, 2007). To take into account the thermal vibration of atoms the frozen-lattice approach can be applied. In this approach, atom configurations with atoms displaced according to the root-mean-square (r.m.s.) displacement are generated and the resulting TEM images are calculated using a multislice approach. The final image is gained by averaging over all the images (Loane *et al.*, 1991). Since the r.m.s. displacement is proportional to the Debye–Waller factor (see §4.1), an accurate knowledge of the r.m.s. displacement or the Debye–Waller factor is required at the temperature prevailing in the experiment.

Experimentally, the Debye–Waller factor can be measured using X-ray diffraction (*e.g.* Stahn *et al.*, 1998) or neutron diffraction. In both techniques it is obtained as a fit parameter. A more direct measurement was performed by Midgley *et al.* (1998) using the electron precession technique. However, experimental values are often published for only a few temperatures. Theoretically, the Debye–Waller factor can be derived using lattice dynamical models (Vetelino *et al.*, 1972) or shell models (Reid, 1983), which rely on fitting model parameters to experimental phonon frequencies. Recently, Gao & Peng (1999) calculated Debye–Waller factors B for 68 elemental crystals from measured phonon densities of states $g(\omega)$ using the equation

$$B = \frac{4\pi^2\hbar}{m}\int_0^\infty \mathrm{d}\omega \coth\left(\frac{\hbar\omega}{2k_\mathrm{B}T}\right)\frac{g(\omega)}{\omega}, \qquad (1)$$

where ω denotes the phonon frequency, T the temperature, m the mass of the atom, $h = 2\pi\hbar$ Planck's constant and k_B Boltzmann's constant. Using a generalization of equation (1), Lee & Gonze (1995) calculated the Debye–Waller factors of SiO_2 and stishovite for a computed phonon density of states. The phonon density of states was derived from a variational density functional perturbation theory. As for measured Debye–Waller factors, calculated Debye–Waller factors are often given for only a few temperatures. In order to provide Debye–Waller factors for the whole temperature range between 0 K and the melting temperature, Sears & Shelley (1991) used an expansion of the coth function in equation (1) that is valid for large and small temperatures. It was found that this approach failed to fit Debye–Waller factors for elemental crystals at intermediate temperatures (Gao & Peng, 1999). Therefore, these authors used different fourth-order polynomials for temperatures below and above 80 K, yielding overall ten fit parameters per material.

In this paper we compute accurate Debye–Waller factors for a variety of group IV, III–V and II–VI semiconductors with the sphalerite crystal structure in the temperature range from

0.1 to 1000 K using a similar approach to that of Lee & Gonze (1995). However, for the computation of phonon densities of states we use the direct method of Parlinski *et al.* (1997). This method is based on the harmonic approximation, which is reviewed briefly in §2. In §3.1 we describe the computation of phonon densities of states for the nonpolar crystals Si, Ge and diamond. In order to take into account polarization effects, Born effective charges were computed. Computation of Born effective charges and their effect on phonon frequencies are described in §3.2. In the final section the calculation of Debye–Waller factors and an efficient fitting approach for Debye–Waller factors are described.

2. Theory of lattice dynamics

In this section we review the theory of lattice dynamics. We follow the derivation of Maradudin (1971) and Cochran & Cowley (1962).

2.1. The equations of motion

In the harmonic approximation the potential energy is expanded in terms of the atomic displacements (and the associated electric fields in case of ionic crystals) up to quadratic terms. Denoting by $\mathbf{u}(m, \mu)$ the displacement of atom μ in the primitive unit cell m from its equilibrium position and by $\mathbf{E}(m, \mu)$ the electric field at atomic position (m, μ), we can write for the potential energy value (taking $H = 0$ at equilibrium) (Cochran & Cowley, 1962)

$$\begin{aligned} H(\mathbf{E}, \mathbf{u}) = {} & \tfrac{1}{2} \sum_{m,\mu;\alpha,\, n,\nu;\beta} \tilde{V}_{\alpha\beta}(m, \mu; n, \nu) u_\alpha(m, \mu) u_\beta(n, \nu) \\ & - \tfrac{1}{2} \sum_{m,\mu;\alpha,\, n,\nu;\beta} \tilde{\chi}_{\alpha\beta}(m, \mu; n, \nu) E_\alpha(m, \mu) E_\beta(n, \nu) \\ & - \sum_{m,\mu;\alpha,\, n,\nu;\beta} \tilde{Z}_{\alpha\beta}(m, \mu; n, \nu) E_\beta(n, \nu) u_\alpha(m, \mu), \end{aligned} \tag{2}$$

where α and β index the components of the displacements $\mathbf{u}$ and of the electric field $\mathbf{E}$. $\tilde{\chi}_{\alpha\beta}(m, \mu; n, \nu)$, $\tilde{V}_{\alpha\beta}(m, \mu; n, \nu)$ and $\tilde{Z}_{\mu;\alpha,\beta}(m, \mu; n, \nu)$ are the elements of the electronic polarizability tensor, the force constant matrix and the transverse effective charge tensor, respectively. They are connected with the second derivatives of the energy by

$$\tilde{\chi}_{\alpha\beta}(m, \mu; n, \nu) = -\left. \frac{\partial^2 H}{\partial E_\alpha(m, \mu)\, \partial E_\beta(n, \nu)} \right|_{\mathbf{E}=\mathbf{0},\, \mathbf{u}=\mathbf{0}}, \tag{3}$$

$$\tilde{V}_{\alpha\beta}(m, \mu; n, \nu) = \left. \frac{\partial^2 H}{\partial u_\alpha(m, \mu)\, \partial u_\beta(n, \nu)} \right|_{\mathbf{E}=\mathbf{0},\, \mathbf{u}=\mathbf{0}}, \tag{4}$$

$$\tilde{Z}_{\alpha,\beta}(m, \mu; n, \nu) = -\left. \frac{\partial^2 H}{\partial E_\alpha(m, \mu)\, \partial u_\beta(n, \nu)} \right|_{\mathbf{E}=\mathbf{0},\, \mathbf{u}=\mathbf{0}}. \tag{5}$$

Since the dipole moment of an atom (m, μ) is given by

$$p_\alpha(m, \mu) = -\partial H / \partial E_\alpha(m, \mu), \tag{6}$$

the transverse effective charge [equation (5)] can be interpreted as the change of dipole moment of an atom (m, μ) due to the displacement of the atom (n, ν). Analogously the electronic polarizability tensor can be interpreted as the change of the dipole moment of an atom (m, μ) due to the electric field acting on the atom (n, ν). Using the energy of the system [equation (2)], the force on an atom (o, Ω) is given by

$$F_\gamma(o, \Omega) = -\partial H / \partial u_\gamma(o, \Omega) \tag{7}$$

and the equation of motion can be found as

$$\begin{aligned} M_\mu \ddot{u}_\alpha(m, \mu) = {} & -\sum_{n,\nu;\beta} \tilde{V}_{\alpha\beta}(m, \mu; n, \nu) u_\beta(n, \nu) \\ & + \sum_{n,\nu;\beta} \tilde{Z}_{\alpha\beta}(m, \mu; n, \nu) E_\beta(n, \nu), \end{aligned} \tag{8}$$

where M_μ is the mass of the atom μ. To simplify the equations of motion, one can exploit the periodicity of the crystal by the *Ansatz*

$$u_\alpha(m, \mu) = [u_\alpha(\mu)/M_\mu] \exp[-i\omega t + 2\pi i \mathbf{k} \cdot \mathbf{r}(m, \mu)], \tag{9}$$

$$E_\alpha(m, \mu) = E_\alpha \exp[-i\omega t + 2\pi i \mathbf{k} \cdot \mathbf{r}(m, \mu)]. \tag{10}$$

Inserting the *Ansatz* into the equation of motion [equation (8)], one finds

$$\begin{aligned} \omega^2(\mathbf{k}) u_\alpha(\mu) = {} & \sum_{\nu,\beta} D^{\mathrm{AN}}_{\alpha\beta}(\mu, \nu; \mathbf{k}) u_\beta(\nu) \\ & - [1/(M_\mu)^{1/2}] \sum_\beta Z_{\alpha\beta}(\mu; \mathbf{k}) E_\beta, \end{aligned} \tag{11}$$

with the analytical part of the dynamical matrix $D^{\mathrm{AN}}_{\alpha\beta}(\mu, \nu; \mathbf{k})$

$$\begin{aligned} D^{\mathrm{AN}}_{\alpha\beta}(\mu, \nu; \mathbf{k}) = {} & \sum_n [\tilde{V}_{\alpha\beta}(m, \mu; n, \nu)/(M_\mu M_\nu)^{1/2}] \\ & \times \exp\{2\pi i \mathbf{k} \cdot [\mathbf{r}(n, \nu) - \mathbf{r}(m, \mu)]\} \end{aligned} \tag{12}$$

and the Born effective charge tensor $Z_{\alpha\beta}(\mu; \mathbf{k})$

$$\begin{aligned} Z_{\alpha\beta}(\mu; \mathbf{k}) = {} & \sum_{n,\nu} \tilde{Z}_{\alpha\beta}(m, \mu; n, \nu) \\ & \times \exp\{2\pi i \mathbf{k} \cdot [\mathbf{r}(n, \nu) - \mathbf{r}(m, \mu)]\}. \end{aligned} \tag{13}$$

2.2. Solution for nonpolar materials

For nonpolar materials, Born effective charges vanish since no polarization is created by the displacement of atoms and, therefore, the last term in equation (8) containing the Born effective charges vanishes as well. Hence, equation (11) becomes

$$\omega^2(\mathbf{k}, \lambda) u_\alpha(\mu; \mathbf{k}, \lambda) = \sum_{\nu,\beta} D^{\mathrm{AN}}_{\alpha\beta}(\mu, \nu; \mathbf{k}) u_\beta(\nu; \mathbf{k}, \lambda), \tag{14}$$

where λ indexes the different eigenvalues of the dynamical matrix $D^{\mathrm{AN}}_{\alpha\beta}(\mu, \nu; \mathbf{k})$.

2.3. Solution for polar materials

For polar materials the last term in equation (8) does not vanish. To derive an eigenvalue equation from equation (8), one needs to express the electric field as a function of the displacements of the atoms. It can be shown [Maradudin (1971), Section VI.2.b] that the electric field is determined by

the component of the macroscopic polarization $\mathbf{P}_\parallel$ parallel to the $\mathbf{k}$ vector of the phonon mode

$$\mathbf{E} = -(1/\varepsilon_0)\mathbf{P}_\parallel, \tag{15}$$

or expressed using the $\mathbf{k}$ vectors

$$E_\alpha = -(1/\varepsilon_0)\sum_\beta \hat{k}_\alpha \hat{k}_\beta P_\beta, \tag{16}$$

where $\hat{k} = \mathbf{k}/|\mathbf{k}|$ is the unit vector in direction of $\mathbf{k}$ and ε_0 is the dielectric constant. The macroscopic polarization is given by

$$P_\gamma = (1/\Omega_0)\sum_{o,\Omega} p_\gamma(o, \Omega), \tag{17}$$

where Ω_0 is the volume of the unit cell and $\mathbf{P}(o, \Omega)$ is the dipole moment of atom (o, Ω) given by equation (6). Inserting equation (2) in equation (6) and substituting the result into equation (17) yields with the *Ansatz* for the dipole moment

$$p_\alpha(m, \mu) = p_\alpha \exp[-i\omega t + 2\pi i \mathbf{k}\cdot\mathbf{r}(m, \mu)] \tag{18}$$

the equation for the macroscopic polarization,

$$P_\alpha = (1/\Omega_0)\sum_{\beta;\mu,\nu} \chi_{\alpha\beta}(\mu, \nu; \mathbf{k})E_\beta + (1/\Omega_0)\sum_{\beta;\mu,\nu} Z_{\alpha\beta}(\mu, \mathbf{k})[u_\beta(\nu)/(M_\nu)^{1/2}]. \tag{19}$$

In equation (19) $\chi_{\alpha\beta}(\mu, \nu; \mathbf{k})$ was defined as

$$\chi_{\alpha\beta}(\mu, \nu; \mathbf{k}) = \sum_n \tilde{\chi}(m, \mu; n, \nu) \times \exp\{2\pi i \mathbf{k}\cdot[\mathbf{r}(n, \nu) - \mathbf{r}(m, \mu)]\}. \tag{20}$$

Combining the polarization in the harmonic approximation equation (19) and equation (16) yields a relation between the electric field and the displacement:

$$E_\gamma = -\frac{\hat{k}_\gamma}{\varepsilon_0\Omega_0\varepsilon_\mathrm{L}^\infty}\sum_{\beta\nu}\left[\sum_\alpha \hat{k}_\alpha Z_{\alpha\beta}(\nu; \mathbf{k})\right]\frac{u_\beta(\nu)}{M_\nu}, \tag{21}$$

where $\varepsilon_\mathrm{L}^\infty$ is given by

$$\varepsilon_\mathrm{L}^\infty = \sum_{\alpha\beta}\hat{k}_\alpha \varepsilon_{\alpha\beta}^\infty \hat{k}_\beta \tag{22}$$

and $\varepsilon_{\alpha\beta}^\infty$ is the dielectric tensor at infinite frequency. Substituting equation (21) into the equation (11) yields

$$\omega^2 u_\alpha(\mu) = \sum_{\nu,\beta}\left[D_{\alpha\beta}^\mathrm{AN}(\mu, \nu; \mathbf{k}) + D_{\alpha\beta}^\mathrm{NA}(\mu, \nu; \mathbf{k})\right]u_\beta(\nu), \tag{23}$$

with the non-analytical part of the dynamical matrix

$$D_{\alpha\beta}^\mathrm{NA}(\mu, \nu; \mathbf{k}) = \frac{\left[\sum_\gamma Z_{\alpha\gamma}(\mu; \mathbf{k})\hat{k}_\gamma\right]\left[\sum_\gamma Z_{\gamma\beta}(\nu; \mathbf{k})\hat{k}_\gamma\right]}{\varepsilon_0\varepsilon_\mathrm{L}^\infty\Omega_0(M_\mu M_\nu)^{1/2}}. \tag{24}$$

3. Computation of dispersion relations

In order to solve the eigenvalue problem equation (23), force-constant matrices, Born effective charges and dielectric tensors have to be computed [equations (12) and (24)]. The computation of the force-constant matrices will be explained in §3.1 and the computation of Born effective charges and dielectric tensors will be explained in §3.2.

3.1. Nonpolar materials

3.1.1. Description of the computational approach. We calculate accurate phonon frequencies from Hellmann–Feynman forces using the direct method of Parlinski *et al.* (1997). The Hellmann–Feynman forces are computed using the full potential linearized augmented plane wave (FPLAPW) code *WIEN2k* (Blaha *et al.*, 2001). In this code the cell is divided into spheres (muffin-tin spheres) around the positions of the atoms. Within the muffin-tin spheres the potential and the wavefunctions are described by atom-like functions and outside the spheres by plane waves. The interstitial wavevector cutoff was set in such a way that $R_\mathrm{MT}K_\mathrm{max} = 7.0$, where K_max is the largest plane-wave vector and R_MT is the radius of the smallest muffin-tin sphere; radii were chosen to obtain nearly touching spheres. The *WIEN2k* code works with periodic boundary conditions.

For equation (2) to be valid we have to expand around the equilibrium position of the atoms. Therefore we first determined the optimal lattice parameter for each semiconductor. In Table 1 experimental lattice parameters (column 4) are compared with lattice parameters that were computed using the local density approximation (LDA) within the parametrization of Perdew & Wang (1992) of the Monte Carlo simulations of Ceperley & Alder (1980) or the generalized gradient approximation (GGA) of Perdew *et al.* (1996) as the exchange and correlation part of the potential (columns 2 and 3). The comparison shows clearly that lattice parameters computed using LDA/GGA are smaller/larger than the experimental lattice parameters, which is in line with the often observed over/under-binding of LDA/GGA.

Using the optimized lattice parameter, a supercell was generated for each inequivalent atom in the asymmetric unit. The inequivalent atoms were displaced by about 4 pm in one direction. Owing to the cubic symmetry of the nonpolar semiconductors it was sufficient to displace the inequivalent atom in the x direction only. In order to get rid of residual forces that arise due to not perfectly optimized lattice parameters, the displacements were performed in positive and negative directions. For each of the supercells described, the Hellmann–Feynman forces due to the displacement of the inequivalent atom on all the other atoms in the supercell were computed using the *WIEN2k* code and symmetrized with respect to the displacements in the opposite directions. From the Hellmann–Feynman forces the corresponding displacement force-constant matrices were derived using the *PHONON* program of Parlinski *et al.* (1997). The force-constant matrices characterize the strength of the bond between two atoms. Dynamical matrices of the crystal [equation (14)] were approximated with the dynamical matrix of the supercell. [For a detailed discussion see Parlinski *et al.* (1997).]

In principle, one should calculate the dynamical matrix of the infinite crystal, but as long as the interaction range is

Table 1
Comparison of the lattice parameter a (Å) computed with the *WIEN2k* code and with the *ABINIT* code using the LDA and the GGA, respectively, with the experimental lattice parameter.

Material	*WIEN2k*		Experimental	*ABINIT*	
	a_{LDA}	a_{GGA}	a_{exp}	a_{LDA}	a_{GGA}
AlN	4.352	4.406	4.380	4.312	4.404
AlP	5.440	5.513	5.467	5.412	5.508
AlAs	5.633	5.732	5.661	5.622	5.749
AlSb	6.116	6.217	6.136	6.076	6.232
GaN	4.460	4.545	4.500	4.321	4.523
GaP	5.396	5.507	5.450	5.321	5.506
GaAs	5.612	5.752	5.654	5.536	5.758
GaSb	6.050	6.214	6.096	5.964	6.207
InN	4.945	5.042	4.980	4.911	5.010
InP	5.831	5.959	5.870	5.824	5.950
InAs	6.038	6.186	6.058	6.016	6.180
InSb	6.448	6.634	6.479	6.419	6.613
MgS	5.604	5.713	5.622	5.582	5.686
MgSe	5.880	6.008	5.890	5.866	5.994
MgTe	6.383	6.524	6.420	6.351	6.502
ZnS	5.313	5.457	5.410	5.335	5.486
ZnSe	5.586	5.746	5.670	5.581	5.779
ZnTe	6.020	6.197	6.103	5.986	6.191
CdS	5.769	5.933	5.820	5.817	5.994
CdSe	6.018	6.197	6.080	6.065	6.264
CdTe	6.422	6.627	6.482	6.424	6.651
C	3.546	3.582	3.567	3.524	3.566
Si	5.408	5.477	5.431	5.384	5.469
Ge	5.626	5.762	5.658	5.577	5.776

confined to the interior of the supercells, the dynamical matrices of the supercells can be used to approximate the dynamical matrices of the infinite crystal. In order to take care that the interaction range was enclosed in the supercell, we always checked that the Hellmann–Feynman forces dropped several orders of magnitude with increasing distance between interacting atoms. The respective phonon frequency $\omega(\mathbf{k}, \lambda)$ for a phonon wavevector $\mathbf{k}$ and branch λ can be derived by solving the eigenvalue problem equation (14) with the dynamical matrix.

3.1.2. Convergence studies for Ge. In the following we will present for Ge studies of the convergence of the phonon frequencies with respect to the number of $\mathbf{k}$ points, the magnitude of the displacement vector and the size of the set of supercells.

Fig. 1 shows the phonon dispersion relation of Ge derived from force constants computed using 100 and 800 $\mathbf{k}$ points in the full Brillouin zone. For the calculation a $1 \times 1 \times 1$ supercell was used. The green line corresponds to 100 $\mathbf{k}$ points and the fat black line surrounding the green line corresponds to 800 $\mathbf{k}$ points. The fact that the black line perfectly surrounds the green line already shows that 100 $\mathbf{k}$ points are sufficient to get a good dispersion relation. For comparison, experimental phonon frequencies (Nilsson & Nelin, 1971) are shown as red dots in Fig. 1.

From Fig. 2, one immediately sees that the magnitude of the displacement vector hardly affects the phonon frequencies. Small deviations are visible only for a rather large displacement of 16 pm. The experimental frequencies (red dots) are taken from Nilsson & Nelin (1971). As already mentioned, the dynamical matrix of the supercell should resemble the dynamical matrix of the whole crystal. Therefore, the phonon

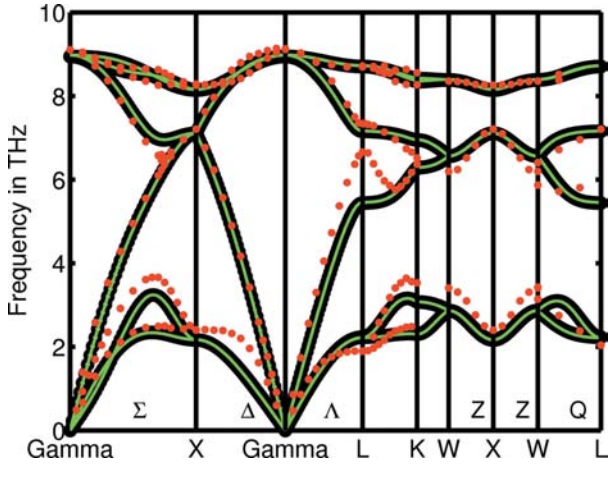

Figure 1
Comparison of phonon dispersion relations of Ge computed within the LDA using different numbers of $\mathbf{k}$ vectors with measured phonon frequencies (red dots). The green (black) curve shows the results using 100 (800) $\mathbf{k}$ points in the full Brillouin zone for the computation of the Hellmann–Feynman forces. The computation was performed on a $1 \times 1 \times 1$ supercell.

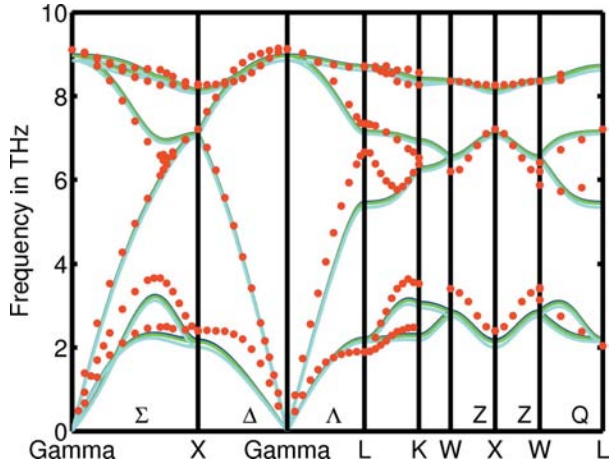

Figure 2
Comparison of the phonon dispersion relation of Ge computed within the LDA for different moduli of the displacement of the inequivalent atoms with measured phonon frequencies (red dots). The black (blue, green, cyan) curve shows the phonon dispersion curve for a displacement of 2 (4, 8, 16) pm.

frequencies should depend on the size of the supercell. Clear deviations from the experimental phonon frequencies can already be observed in Figs. 1 and 2, *e.g.* close to the *L* point. In Fig. 3, phonon dispersion relations computed from $1 \times 1 \times 1$, $2 \times 2 \times 2$ and $3 \times 3 \times 3$ supercells are compared with a measured phonon dispersion relation (Nilsson & Nelin, 1971). For the $1 \times 1 \times 1$ supercell significant deviations from the measured phonon frequencies can be observed, but already the $2 \times 2 \times 2$ supercell shows reasonable agreement between measurement and experiment. The agreement is even better for the $3 \times 3 \times 3$ supercell. However, due to the high computational effort of the large $3 \times 3 \times 3$ supercell we restricted the calculations to $2 \times 2 \times 2$ supercells.

3.2. Polar semiconductors

3.2.1. Description of the computational approach. In order to take into account polarization, knowledge of Born effective charges and dielectric tensors is needed [see equation (24)]. We computed both using the *ABINIT* code (Gonze *et al.*, 2002). The *ABINIT* code allows the computation of Born effective charges and dielectric tensors based on a variational density functional perturbation theory approach (Gonze & Lee, 1997). In contrast to the *WIEN2k* code, the *ABINIT* code is not an all-electron code and therefore uses pseudopotentials in the vicinity of the cores of the atoms. We used norm-conserving pseudopotentials generated according to the Troullier–Martins scheme (Troullier & Martins, 1991) with the *FHI* code provided on the web page of the *ABINIT* code at http://www.abinit.org.

We started the computation of Born effective charges and dielectric tensors by optimization of the lattice parameters using the *ABINIT* code. We computed total energies for a series of lattice parameters. Total energies were fitted in the vicinity of their minima using a parabola. The minima were used as the lattice parameters for the computation of Born effective charges and dielectric tensors. These lattice parameters are found in columns 5 and 6 in Table 1. Typically, lattice parameters were overestimated by approximately 1.5% when the GGA was used and they were underestimated by 1.2% when the LDA was used. (We used the same parametrizations of the exchange and correlation potentials for computations in *ABINIT* as for computations in *WIEN2k*.) Using the optimized lattice parameters we computed Born effective charges for different energy cutoffs of the plane-wave expansion. For most materials, an energy cutoff of about 24 *Ha* was sufficient to converge the Born effective charges to at least three digits. To check the quality of the convergence of the computation several sum rules can be checked: according to Gonze & Lee (1997) the charge neutrality in one unit cell must also be fulfilled for the Born effective charges, *i.e.*

$$\sum_{\mu} Z_{\alpha\beta}(\mu; \mathbf{k}) = 0. \tag{25}$$

Another rule that can be checked within the *ABINIT* code is the f-sum rule, which should result in 1 (Gonze & Lee, 1997).

In Tables 2 and 3 the computed Born effective charges for $\mathbf{k} = 0$ and dielectric constants computed within the LDA and the GGA, respectively, are given. The Born effective charges are given for both anions and cations to show the fulfilment of the sum rule for Born effective charges [equation (25)]. Additionally, the difference $\Delta_{\text{f-sum}}$ of the obtained f-sum rule from 1 is also displayed. The deviation from the f-sum rule $|\Delta_{\text{f-sum}}|$ was for most materials below 3×10^{-4} apart from the Zn compounds and InN. Therefore, further computation using cutoff energies up to about 40 *Ha* were performed for these two materials resulting in the Born effective charges and the $\Delta_{\text{f-sum}}$ values given in the tables for these materials.

Our results are compared with experimental and calculated values (de Gironcoli *et al.*, 1989) for a series of III–V semiconductors in Figs. 4 and 5. Fig. 4 shows Born effective charges computed using the LDA and the GGA as a function of measured Born effective charges. From this figure it becomes evident that our computations within the LDA are situated closer to the experimental values than the LDA computations of de Gironcoli *et al.*, but a larger difference between our GGA values and the experimental ones can be observed. A similar plot for the dielectric constants is shown in Fig. 5. Deviations between experimental values and our computed values can be observed. The deviations are partly caused by the approximation of the exchange and correlation part of the potential, which is not known exactly. This statement is supported by the fact that the values that were computed with different approximations for the exchange and correlation potentials deviate significantly for the same materials (compare the LDA and GGA values in Fig. 5). Another reason is the choice of pseudopotentials, which approximate the potential in the regions close to the atom cores. Comparison of the results of de Gironcoli *et al.* with ours shows that the values that were computed using different pseudopotentials deviate as well (compare the LDA and de Gironcoli *et al.* values).

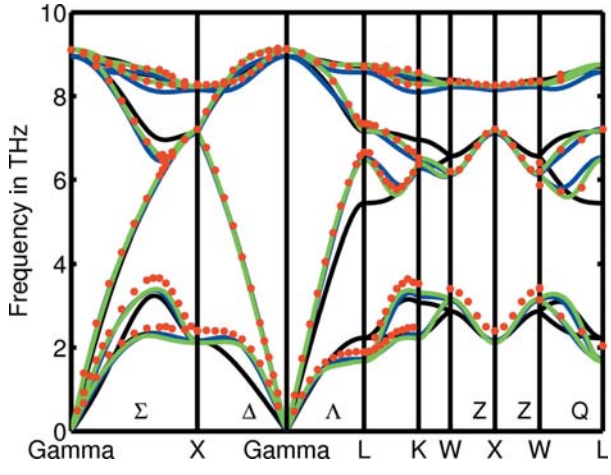

Figure 3
Comparison of the phonon dispersion relation of Ge computed within the LDA for different supercell sizes with measured phonon frequencies (red dots). The black (blue, green) curve shows the phonon dispersion curves for a $1 \times 1 \times 1$ ($2 \times 2 \times 2$, $3 \times 3 \times 3$) supercell. The computed phonon frequencies become more accurate for larger supercells.

Table 2
Born effective charges for **k** = 0 and dielectric constants calculated using the LDA as the exchange and correlation part of the potential.

The residuum between the computed sum rule and 1 is also given, which reflects the precision of the calculation.

Material	Z_{cation}	Z_{anion}	ε_∞	$\Delta_{f\text{-sum}}$
AlN	2.54	−2.54	4.47	6.8e−6
AlP	2.22	−2.22	8.31	−1.3e−5
AlAs	2.13	−2.13	9.38	2.8e−8
AlSb	1.82	−1.82	11.62	−1.6e−5
GaN	2.64	−2.64	4.97	7.6e−6
GaP	2.1	−2.1	10.01	−1.5e−5
GaAs	2.05	−2.05	12.25	−5.8e−6
GaSb	1.62	−1.62	16.36	4.5e−5
InN	2.95	−2.94	12.04	−2.1e−5
InP	2.56	−2.56	11.32	−6.0e−5
InAs	2.57	−2.57	17.39	1.8e−4
InSb	2.24	−2.24	20.05	2.6e−4
MgS	1.85	−1.85	4.15	−1.2e−5
MgSe	1.86	−1.86	4.74	−2.2e−5
MgTe	1.88	−1.88	5.68	−2.1e−5
ZnS	1.96	−1.96	6.36	−5.5e−5
ZnSe	2	−1.99	7.63	−5.8e−5
ZnTe	1.92	−1.91	9.53	−5.8e−5
CdS	2.23	−2.23	7.05	−7.1e−5
CdSe	2.3	−2.29	9.06	−9.4e−5
CdTe	2.19	−2.19	9.92	−8.3e−5
C	0	0	5.71	−1.4e−5
Si	0	0	13.18	1.5e−6
Ge	0	0	19.50	2.8e−4

Table 3
Born effective charges for **k** = 0 and dielectric constants calculated using the GGA as the exchange and correlation part of the potential.

The residuum between the computed sum rule and 1 is also given, which reflects the precision of the calculation.

Material	Z_{cation}	Z_{anion}	ε_∞	$\Delta_{f\text{-sum}}$
AlN	2.55	−2.54	4.59	3.6e−7
AlP	2.25	−2.25	8.14	−1.4e−5
AlAs	2.15	−2.15	9.63	−3.8e−7
AlSb	1.85	−1.85	12.29	−2.0e−5
GaN	2.71	−2.71	5.69	3.4e−6
GaP	2.32	−2.32	10.44	−1.9e−5
GaAs	2.30	−2.30	14.83	−3.6e−6
GaSb	1.95	−1.96	22.47	3.3e−4
InN	2.98	−2.97	14.37	4.5e−5
InP	2.67	−2.67	11.54	−6.9e−5
InAs	2.71	−2.70	20.33	2.5e−4
InSb	2.45	−2.44	25.57	4.2e−4
MgS	1.89	−1.89	4.01	−1.5e−5
MgSe	1.90	−1.90	4.63	−2.1e−5
MgTe	1.94	−1.93	5.56	−1.9e−5
ZnS	2.08	−2.08	6.12	−5.7e−5
ZnSe	2.16	−2.16	7.57	−6.3e−5
ZnTe	2.13	−2.12	9.51	−6.4e−5
CdS	2.32	−2.32	6.60	−7.6e−5
CdSe	2.40	−2.40	8.57	−9.6e−5
CdTe	2.37	−2.37	9.75	−9.2e−5
C	0	0	5.80	−1.7e−5
Si	0	0	13.05	1.6e−6
Ge	0	0	29.07	1.0e−3

3.2.2. Phonon dispersion relations of polar materials. Fig. 6 compares computed (LDA) phonon dispersion relations for GaAs with experimental phonon frequencies taken from Strauch & Dorner (1990). The computations were first carried out taking into account the polarization in the crystal (black line) and then the polarization was neglected by setting the Born effective charges to zero (green line). For the computation of the Hellmann–Feynman forces 2 × 2 × 2 supercells were used and the inequivalent atoms were displaced by 4 pm (see also §3.1.2). From Fig. 6 it can be seen that due to the polarization the optical phonons split into two different branches at the centre of the Brillouin zone (Γ point), *i.e.* the splitting of the longitudinal optical mode and the transverse optical modes (LO–TO splitting). The calculation where the polarization is taken into account better resembles the experimental phonon frequencies.

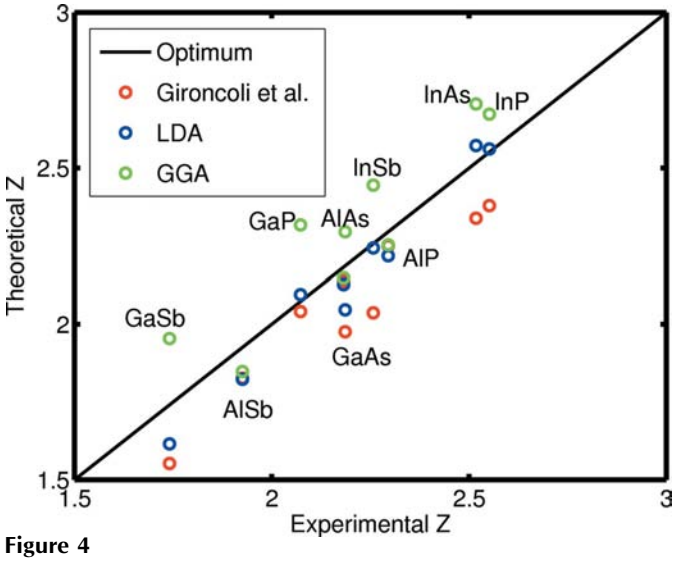

Figure 4
Computed absolute values of Born effective charges for some III–V semiconductors plotted *versus* experimental values taken from de Gironcoli *et al.* (1989). Born effective charges computed using the LDA (GGA) are shown in blue (green). The values are compared to the computed values of de Gironcoli *et al.* (1989) (red circles).

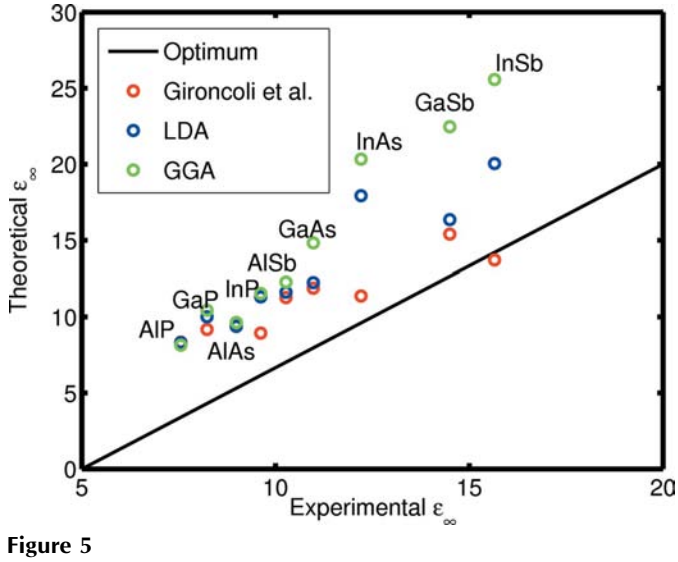

Figure 5
Computed ε_∞ for some III–V semiconductors plotted *versus* experimental values taken from de Gironcoli *et al.* (1989). ε_∞ computed using the LDA (GGA) are shown in blue (green). The values are compared to the computed values of de Gironcoli *et al.* (1989) (red circles).

4. Calculation of Debye–Waller factors

In this section the calculation of Debye–Waller factors is described. We use a generalized form of equation (1). Therefore, we review in §4.1 how the generalized form of equation (1) can be derived. In §§4.2 and 4.3 we describe the calculation of Debye–Waller factors and the fitting procedure.

4.1. Generalized phonon density of states and Debye–Waller factor

For TEM simulations the Coulomb potential of the material under investigation is needed and usually the Coulomb potential is written as a Fourier series with Fourier components V^{hkl} calculated as

$$V^{hkl} \propto \sum_{\nu} f_{\nu}^{hkl} \exp[2\pi i \mathbf{g}^{hkl} \cdot \mathbf{r}(\nu)], \tag{26}$$

where f_{ν}^{hkl} are the atomic scattering factors for atom ν and the reflection g^{hkl}. Atomic scattering factors are typically taken from *e.g.* Doyle & Turner (1968) or Weickenmeier & Kohl (1991). However, such a potential is unrealistic and does not even correspond to the potential at a temperature of 0 K because of the zero-point motion of the atoms. In order to take into account a finite temperature of the system, one can assume a time-dependent potential (Kittel, 1988). Then the position of the atom $\mathbf{r}(\nu)$ becomes time dependent and we substitute $\mathbf{r}(\nu)$ by $\mathbf{r}(\nu, t) = \mathbf{r}(\nu) + \mathbf{u}(\nu, t)$ with $\mathbf{u}(\nu, t)$ being the displacement of the atom from its equilibrium position. Averaging the potential over time yields

$$\langle V^{hkl} \rangle_t \propto \sum_{\nu} f_{\nu}^{hkl} \exp[2\pi i \mathbf{g}^{hkl} \cdot \mathbf{r}(\nu)] \langle \exp[2\pi i \mathbf{g}^{hkl} \cdot \mathbf{u}(\nu, t)] \rangle_t, \tag{27}$$

where the index t denotes that the averaging is performed over time. Following the derivation in Kittel (1988), we find

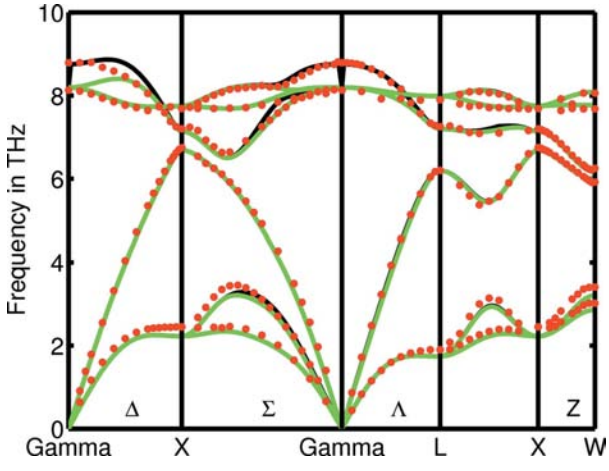

Figure 6
Comparison of phonon dispersion relations for GaAs with experimental phonon frequencies. The black line shows the result where the polarization was taken into account using the computed Born effective charges. The green line shows the result when the polarization is neglected, *i.e.* the Born effective charges have been assumed to be zero.

$$\langle V^{hkl} \rangle_t \propto \sum_{\nu} f_{\nu}^{hkl} \exp[2\pi i \mathbf{g}^{hkl} \cdot \mathbf{r}(\nu)] \times \exp\left[-2\pi^2 \sum_{\alpha\beta} g_{\alpha}^{hkl} \langle u_{\alpha}(\nu, t) u_{\beta}(\nu, t) \rangle_t g_{\beta}^{hkl}\right]. \tag{28}$$

In the following we will focus on the quantity $\langle u_{\alpha}(\nu, t) u_{\beta}(\nu, t) \rangle_t$, which equals the static correlation function $\langle u_{\alpha}(\nu) u_{\beta}(\nu) \rangle$ because of the time translation invariance. Using the ergodic hypothesis we replace the time average by an ensemble average. The static correlation function can be derived by expanding the displacements into the normal coordinates $Q(\mathbf{k}, \lambda)$,

$$u_{\alpha}(m, \mu) = \frac{1}{N(M_{\mu})^{1/2}} \sum_{\mathbf{k},\lambda} u_{\alpha}(\mu; \mathbf{k}, \lambda) \exp[2\pi i \mathbf{k} \cdot \mathbf{r}(m)] Q(\mathbf{k}, \lambda). \tag{29}$$

Using this expansion for building up the Lagrangian of the system yields a harmonic oscillator equation for the normal coordinates:

$$\ddot{Q}(\mathbf{k}, \lambda) + \omega^2(\mathbf{k}, \lambda) Q(\mathbf{k}, \lambda) = 0. \tag{30}$$

Interpreting now the normal coordinates $Q(\mathbf{k}, \lambda)$ as quantum-mechanical operators and writing them in terms of creation and annihilation operators yields

$$Q(\mathbf{k}, \lambda) = [\hbar/2\omega(\mathbf{k}, \lambda)]^{1/2} [a(\mathbf{k}, \lambda) + a^{\dagger}(\mathbf{k}, \lambda)]. \tag{31}$$

Using the expansion equation (29) one can find for the correlation function

$$\langle u_{\alpha}(\nu) u_{\beta}(\nu) \rangle = \frac{\hbar}{4NM_{\nu}} \sum_{\mathbf{k},\lambda} \frac{e_{\alpha}(\nu; \mathbf{k}, \lambda) e_{\beta}^{*}(\nu; \mathbf{k}, \lambda)}{\omega(\mathbf{k}, \lambda)} [\overline{n}(\mathbf{k}, \lambda) + \tfrac{1}{2}], \tag{32}$$

where $\overline{n}(\mathbf{k}, \lambda) = \langle a(\mathbf{k}, \lambda) a^{\dagger}(\mathbf{k}, \lambda) \rangle$ is the average number of phonons in the mode characterized by the wavevector $\mathbf{k}$ and branch λ. The average number of phonons $\overline{n}(\mathbf{k}, \lambda)$ is given by the Bose–Einstein distribution

$$\overline{n}(\mathbf{k}, \lambda) = \frac{1}{\exp[\hbar\omega(\mathbf{k}, \lambda)/(k_{\mathrm{B}} T)] - 1}. \tag{33}$$

Substituting the Bose–Einstein distribution equation (33) into equation (32) yields for the static correlation function

$$\langle u_{\alpha}(\nu) u_{\beta}(\nu) \rangle = \frac{\hbar}{2NM_{\nu}} \sum_{\mathbf{k},\lambda} \frac{e_{\alpha}(\nu; \mathbf{k}, \lambda) e_{\beta}^{*}(\nu; \mathbf{k}, \lambda)}{\omega(\mathbf{k}, \lambda)} \times \coth\left[\frac{\hbar\omega(\mathbf{k}, \lambda)}{2k_{\mathrm{B}} T}\right]. \tag{34}$$

Introducing an integral over the frequency, equation (34) can be rewritten as

$$\langle u_{\alpha}(\nu) u_{\beta}(\nu) \rangle = \frac{\hbar r}{2M_{\nu}} \int_0^{\infty} \mathrm{d}\omega \frac{\coth(\hbar\omega/2k_{\mathrm{B}} T)}{\omega} g_{\alpha\beta}(\nu; \omega), \tag{35}$$

where r is the number of phonon branches and $g_{\alpha\beta}(\nu; \omega)$ is the generalized phonon density of states given by

$$g_{\alpha\beta}(\nu;\omega) = (1/\Delta\omega r)\sum_{\mathbf{k},\lambda} e_\alpha(\nu;\mathbf{k},\lambda)e^*_\beta(\nu;\mathbf{k},\lambda)\delta_{\Delta\omega}[\omega-\omega(\mathbf{k},\lambda)], \tag{36}$$

with N the number of phonon wavevectors $\mathbf{k}$ and $\Delta\omega$ the width of the frequency channel of the function $\delta_{\Delta\omega}(\omega)$ that is defined as

$$\delta_{\Delta\omega}(\omega) = \begin{cases} 1 & -\Delta\omega/2 < \omega \leq \Delta\omega/2 \\ 0 & \text{otherwise} \end{cases}. \tag{37}$$

On comparing equation (1) with equation (35) one can easily see the similarity between the equations. The advantage of equation (35) is that one can derive static correlation functions for all atoms in polyatomic materials such as the III–V and II–VI semiconductors. In general, the static correlation function is a matrix for each atom. However, in the case of the cubic materials under investigation here, the diagonal terms should be the same and the off-diagonal terms should be zero. Therefore, the matrix of the static correlation function is just a scalar value for each atom, often called also the r.m.s. displacement.

The relation between the Debye–Waller factor $B_{\alpha\beta}(\nu)$ and the correlation function $\langle u_\alpha(\nu)u_\beta(\nu)\rangle$ follows from writing the exponential damping factor in equation (28) as $\exp[-\frac{1}{4}\mathbf{g}\boldsymbol{B}(\nu)\mathbf{g}]$:

$$B_{\alpha\beta}(\nu) = 8\pi^2\langle u_\alpha(\nu)u_\beta(\nu)\rangle. \tag{38}$$

Note that in our derivations we defined vectors in reciprocal space as $|\mathbf{g}| = 1/d$, where d is a distance in real space.

4.2. Calculation of Debye–Waller factors

To calculate Debye–Waller factors we first calculated generalized phonon densities of states. From the definition of the generalized phonon density of states [equation (36)] one can see that there are two quantities that are not predetermined. These are the number of phonon wavevectors and the frequency channel width $\Delta\omega$ [see equation (37)] in which the phonon energies are sorted when the generalized phonon density of states is evaluated. The convergence studies with respect to the frequency channel width and the number of $\mathbf{k}$ vectors is done for the example of Ge in the following.

Fig. 7 shows a comparison of phonon densities of states, which were derived using a channel width of $\Delta\omega$ = 0.1 THz and different numbers N of phonon $\mathbf{k}$ vectors. The number of $\mathbf{k}$ vectors was increased from 100 to 800 then to 3200. The phonon density of states becomes less and less noisy on increasing the number of $\mathbf{k}$ vectors. In Fig. 8 different phonon density of states are shown for which the frequency channel width varied. The number of phonon $\mathbf{k}$ vectors for each channel width was optimized in a similar way as in Fig. 7. Note that many more $\mathbf{k}$ points were needed for smaller frequency channel widths. The number of $\mathbf{k}$ points used for the calculation of the phonon density of states with a frequency channel width of 0.01 THz was 64 000. The frequency channel widths were 0.5, 0.1, 0.05 and 0.01 THz. It becomes clear that in order to get the high peak at the optical phonons a width of 0.01 THz has to be used. For the different components of the generalized phonon density of states similar results were found.

We also checked the convergence of the Debye–Waller factors with respect to the number of $\mathbf{k}$ points and the frequency channel width. For the optimized number of $\mathbf{k}$ points for the channel widths of 0.05 and 0.01 THz we found that the Debye–Waller factors computed using these channel widths deviated by about 0.054% for Ga and about 0.066% for As at a temperature of about 300 K.

Fig. 9 shows the static correlation function $\langle u_1u_1\rangle$ computed from the g_{11} component of the generalized phonon density of states using equation (35) and a frequency channel width $\Delta\omega$ = 0.5 THz for different numbers of $\mathbf{k}$ vectors. With increasing number of $\mathbf{k}$ vectors the static correlation functions g_{11} lie closer together. In Fig. 10 the 11, 22 and 33 components of the

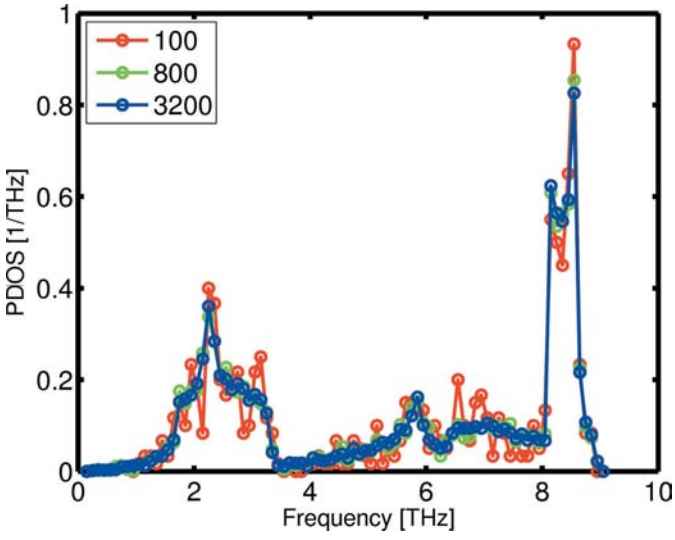

Figure 7
Comparison of phonon density of states (PDOS) for Ge calculated for different numbers of phonon wavevectors $\mathbf{k}$ for a width of the frequency channel of 0.1 THz.

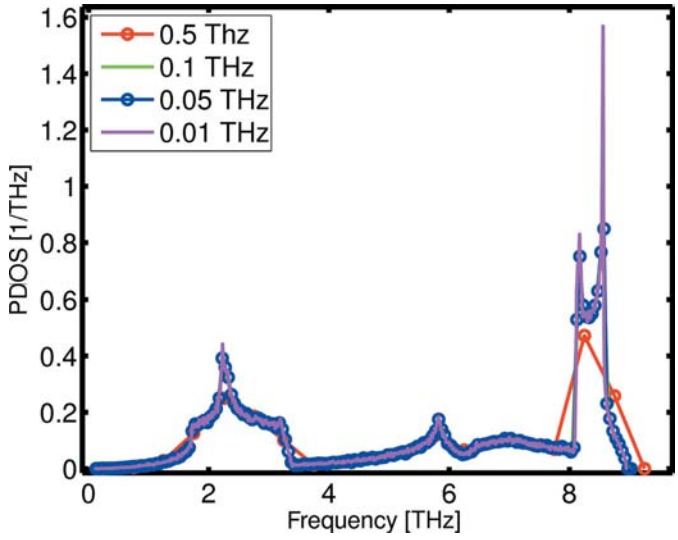

Figure 8
Comparison of phonon density of states (PDOS) for Ge calculated for different frequency channel widths. The number of phonon wavevectors was converged for each phonon frequency channel.

static correlation function are compared for a calculation where frequency channel widths of 0.01 and 0.5 THz were used. For the two different frequency channel widths the number of phonon **k** vectors was optimized as discussed above. One can see that the different components for a channel width of 0.5 THz deviate clearly from each other. The deviation increases with increasing temperature. Note that due to symmetry all the components should be the same. For the frequency channel width of 0.01 THz deviations can hardly be detected in Fig. 10. For the calculation of the Debye–Waller factors for the other materials we took a frequency channel width of 0.01 THz and 100 000 **k** points. We always checked that the deviations between the different components of the Debye–Waller factors at the maximum temperature of 1000 K were smaller than 0.1%.

4.3. Parametrizing the Debye–Waller factors

In the following we describe how we fitted the temperature dependence of the static correlation functions to a model curve. For the contribution of phonons *e.g.* to the specific heat one usually uses the Einstein model for the phonon density of states (Einstein, 1911). The Einstein model mainly describes the optical phonons, since it approximates the phonon density

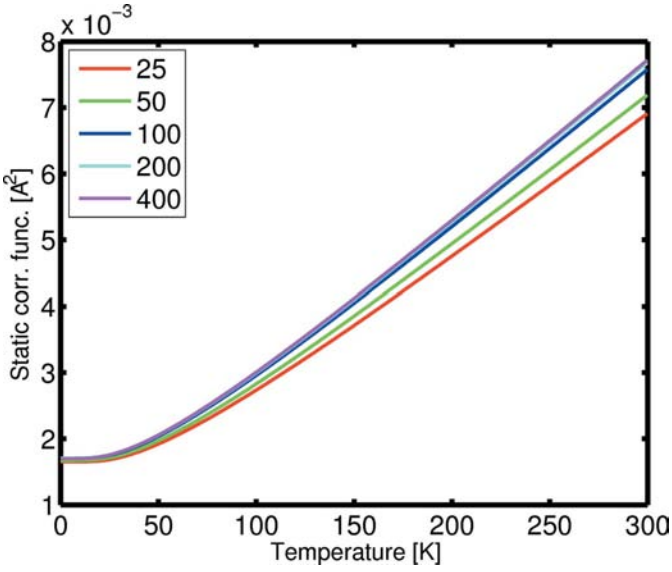

Figure 9
Static correlation function $\langle u_1 u_1 \rangle$ as a function of the temperature calculated from generalized phonon density of states derived for a channel width of 0.5 THz and for different numbers of phonon **k** vectors.

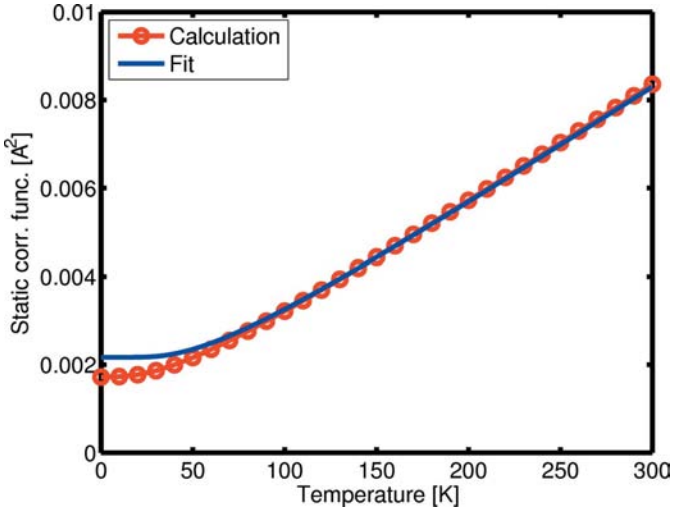

Figure 11
Static correlation function $\langle u_1 u_1 \rangle$ as a function of temperature for Ge and the corresponding fit with the Einstein model for the phonon density of states. The static correlation function is well fitted for temperatures above 100 K, but for temperatures below 100 K clear discrepancies between the fit and the calculated values can be observed.

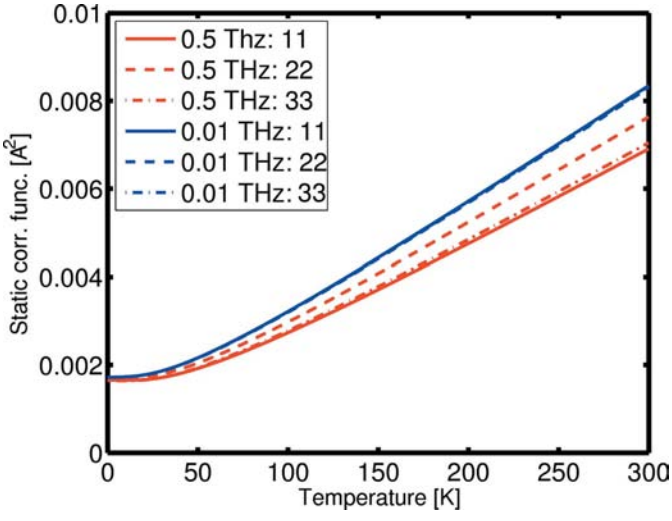

Figure 10
Static correlation function $\langle u_1 u_1 \rangle$ as a function of the temperature calculated from generalized phonon density of states derived for different channel widths for an optimized number of phonon **k** vectors.

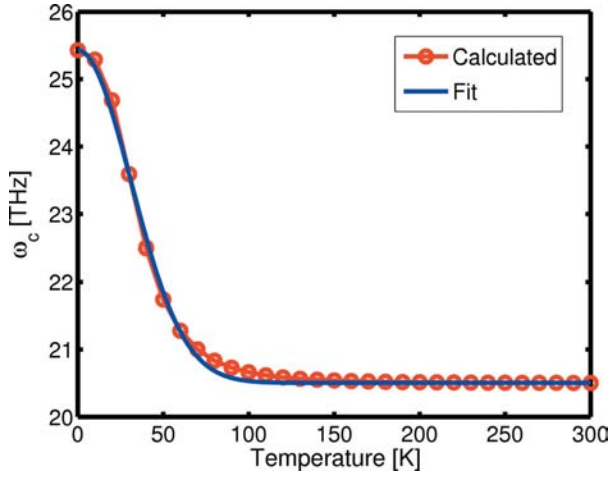

Figure 12
Temperature dependence of the characteristic frequency ω_c. The blue line is a fit with a Gaussian to the characteristic frequency. The fit shows some small deviations, which are not crucial, since they do not affect the fit of the static correlation function very much (see Fig. 13).

Table 4
Fit parameters for the temperature dependence of the characteristic frequency ω_c derived from Hellmann–Feynman forces computed using the LDA.

Material	Element	A	B	σ
AlN	Al	7.516651e+012	6.132446e+013	1.285515e+002
	N	1.479155e+013	8.570636e+013	1.654690e+002
AlP	Al	7.386804e+012	3.608380e+013	7.785658e+001
	P	7.193599e+012	3.543605e+013	7.580339e+001
AlAs	Al	9.644435e+012	3.337473e+013	6.719608e+001
	As	3.193684e+012	2.101611e+013	4.676239e+001
AlSb	Al	1.080553e+013	2.830932e+013	5.446165e+001
	Sb	2.035262e+012	1.397949e+013	3.124928e+001
GaN	Ga	3.584761e+012	3.511461e+013	7.602315e+001
	N	2.046591e+013	8.103009e+013	1.451238e+002
GaP	Ga	3.118889e+012	2.273464e+013	5.118278e+001
	P	1.035200e+013	3.687135e+013	7.262717e+001
GaAs	Ga	4.155864e+012	2.035401e+013	4.479912e+001
	As	4.774990e+012	2.119684e+013	4.544807e+001
GaSb	Ga	4.718997e+012	1.735948e+013	3.728892e+001
	Sb	2.910703e+012	1.412438e+013	3.162801e+001
InN	In	2.465003e+012	2.138380e+013	4.718032e+001
	N	2.380055e+013	6.237666e+013	1.085171e+002
InP	In	1.920652e+012	1.479984e+013	3.447010e+001
	P	1.167324e+013	3.091414e+013	5.888034e+001
InAs	In	2.496191e+012	1.300065e+013	3.026860e+001
	As	5.458328e+012	1.748737e+013	3.689434e+001
InSb	In	2.922115e+012	1.120398e+013	2.559933e+001
	Sb	3.392591e+012	1.173299e+013	2.609895e+001
MgS	Mg	3.358631e+013	2.382342e+013	3.202308e+001
	S	3.756643e+013	1.668628e+013	2.195164e+001
MgSe	Mg	2.427056e+013	2.616853e+013	3.740816e+001
	Se	2.261965e+013	1.273507e+013	1.974979e+001
MgTe	Mg	9.088783e+012	2.311195e+013	4.466514e+001
	Te	1.478982e+012	1.085741e+013	2.508424e+001
ZnS	Zn	2.700108e+012	2.042631e+013	4.671562e+001
	S	9.558977e+012	3.335897e+013	6.587750e+001
ZnSe	Zn	3.574733e+012	1.826960e+013	4.072422e+001
	Se	4.331065e+012	1.906187e+013	4.108036e+001
ZnTe	Zn	4.084093e+012	1.650445e+013	3.557737e+001
	Te	2.716218e+012	1.351366e+013	3.013417e+001
CdS	Cd	1.681754e+012	1.216706e+013	2.911171e+001
	S	1.128410e+013	2.585141e+013	4.959817e+001
CdSe	Cd	2.183634e+012	1.087505e+013	2.600495e+001
	Se	5.094080e+012	1.477335e+013	3.164524e+001
CdTe	Cd	2.467077e+012	1.006627e+013	2.339060e+001
	Te	3.146102e+012	1.078845e+013	2.410573e+001
C	C	1.697695e+013	1.470958e+014	2.798910e+002
Si	Si	8.249187e+012	3.749824e+013	7.990406e+001
Ge	Ge	4.860505e+012	2.060473e+013	4.442509e+001

Table 5
Fit parameters for the temperature dependence of the characteristic frequency ω_c derived from Hellmann–Feynman forces computed using the GGA.

Material	Element	A	B	σ
AlN	Al	7.126538e+012	5.989830e+013	1.253481e+002
	N	1.399117e+013	8.387930e+013	1.614885e+002
AlP	Al	7.451218e+012	3.530067e+013	7.426703e+001
	P	7.455530e+012	3.480381e+013	7.238263e+001
AlAs	Al	9.002114e+012	3.322708e+013	6.673131e+001
	As	3.078957e+012	2.107757e+013	4.656689e+001
AlSb	Al	1.030702e+013	2.815009e+013	5.417596e+001
	Sb	1.976805e+012	1.396697e+013	3.120939e+001
GaN	Ga	3.294616e+012	3.367822e+013	7.288966e+001
	N	1.856878e+013	7.790741e+013	1.391941e+002
GaP	Ga	2.937376e+012	2.220311e+013	4.978109e+001
	P	9.798406e+012	3.626020e+013	7.095718e+001
GaAs	Ga	3.749035e+012	1.944495e+013	4.274642e+001
	As	4.431789e+012	2.048469e+013	4.360005e+001
GaSb	Ga	4.271114e+012	1.648987e+013	3.531536e+001
	Sb	2.717532e+012	1.354364e+013	3.003625e+001
InN	In	2.210383e+012	2.062922e+013	4.539599e+001
	N	2.089763e+013	6.025402e+013	1.045041e+002
InP	In	1.819756e+012	1.449039e+013	3.370622e+001
	P	1.101337e+013	3.042639e+013	5.772974e+001
InAs	In	2.311641e+012	1.252242e+013	2.919999e+001
	As	5.109508e+012	1.696141e+013	3.568273e+001
InSb	In	2.531195e+012	1.089449e+013	2.476549e+001
	Sb	3.048071e+012	1.158120e+013	2.541961e+001
MgS	Mg	3.368866e+013	1.804278e+013	2.221087e+001
	S	3.556272e+013	1.315734e+013	1.575921e+001
MgSe	Mg	2.525422e+013	2.111280e+013	2.867660e+001
	Se	2.181639e+013	9.347292e+012	1.241036e+001
MgTe	Mg	8.195843e+012	2.307651e+013	4.442016e+001
	Te	1.459614e+012	1.099478e+013	2.494851e+001
ZnS	Zn	2.365691e+012	1.941894e+013	4.432231e+001
	S	8.556468e+012	3.228860e+013	6.309353e+001
ZnSe	Zn	3.099511e+012	1.716127e+013	3.827153e+001
	Se	3.959340e+012	1.828798e+013	3.899340e+001
ZnTe	Zn	3.514113e+012	1.546216e+013	3.346367e+001
	Te	2.469776e+012	1.293880e+013	2.865071e+001
CdS	Cd	1.537492e+012	1.185226e+013	2.795118e+001
	S	1.009356e+013	2.541131e+013	4.813208e+001
CdSe	Cd	1.909526e+012	1.060040e+013	2.523488e+001
	Se	4.589196e+012	1.464986e+013	3.097980e+001
CdTe	Cd	1.826297e+012	1.527735e+013	2.902601e+001
	Te	1.536967e+012	1.400198e+013	2.692230e+001
C	C	1.643526e+013	1.444227e+014	2.742977e+002
Si	Si	7.955010e+012	3.801102e+013	8.020465e+001
Ge	Ge	4.557722e+012	1.980667e+013	4.247595e+001

of states by a delta function at the Einstein frequency ω_E. Using the Einstein model of the phonon density of states yields for the static correlation function equation (35)

$$\langle u^2(\nu; T)\rangle = \frac{\hbar}{2M_\nu}\frac{\coth[\hbar\omega_E(\nu)/2k_BT]}{\omega_E(\nu)}, \qquad (39)$$

where we assumed that the different diagonal components of the static correlation function were all the same and the off-diagonal elements are zero. Fig. 11 compares the static correlation function calculated for Ge with a fit using the Einstein model. For the fit we assumed the Einstein frequency $\omega_E(\nu)$ as a fit variable. For higher temperatures the temperature dependence of the static correlation function is very good, but for lower temperatures some deviations occur. Therefore, we solve the integral in equation (35) formally by using the mean-value theorem and exploit the normalization of the phonon density of states. This yields

$$\langle u^2(\nu; T)\rangle = \frac{\hbar}{2M_\nu}\frac{\coth[\hbar\omega_c(\nu; T)/2k_BT]}{\omega_c(\nu, T)}, \qquad (40)$$

where now the Einstein frequency is substituted by the characteristic frequency, which is temperature dependent. The temperature dependence of the characteristic frequency is shown in Fig. 12. We fit the temperature dependence of the characteristic frequency using the Gaussian

$$\omega_c(\nu; T) = A\exp(-T^2/\sigma^2) + B, \qquad (41)$$

yielding three fit parameters: A, B and σ. The fit of the characteristic frequency with the Gaussian is shown in Fig. 12 as well. One can clearly see that the fit is not perfect. However, it is not our intention to fit the characteristic frequency, but the

Table 6
Mean-square displacements $\langle u^2(\nu; T)\rangle$ (Å^2) for selected temperatures computed within the LDA for III–V and group IV materials and within the GGA for II–VI materials.

		Temperature (K)						
Material	Element	0.001	100	200	400	600	800	1000
AlN	Al	1.710e−3	1.827e−3	2.284e−3	3.636e−3	5.161e−3	6.741e−3	8.343e−3
	N	2.256e−3	2.359e−3	2.727e−3	3.897e−3	5.313e−3	6.819e−3	8.368e−3
AlP	Al	2.707e−3	3.527e−3	5.421e−3	9.833e−3	0.014448	0.01912	0.023817
	P	2.405e−3	3.159e−3	4.877e−3	8.87e−3	0.013042	0.017264	0.021508
AlAs	Al	2.736e−3	3.932e−3	6.225e−3	0.011433	0.016847	0.022319	0.027815
	As	1.751e−3	2.999e−3	5.287e−3	0.010184	0.015165	0.020168	0.02518
AlSb	Al	3.009e−3	5.047e−3	8.391e−3	0.015749	0.023319	0.030948	0.038601
	Sb	1.629e−3	3.808e−3	7.152e−3	0.014061	0.021023	0.027998	0.034979
GaN	Ga	1.177e−3	1.452e−3	2.208e−3	4.011e−3	5.899e−3	7.809e−3	9.729e−3
	N	2.234e−3	2.427e−3	2.916e−3	4.282e−3	5.889e−3	7.587e−3	9.328e−3
GaP	Ga	1.762e−3	2.825e−3	4.895e−3	9.373e−3	0.01394	0.01853	0.02313
	P	2.171e−3	2.966e−3	4.547e−3	8.217e−3	0.012063	0.015959	0.019876
GaAs	Ga	1.858e−3	3.397e−3	6.038e−3	0.011658	0.017368	0.023101	0.028844
	As	1.632e−3	2.949e−3	5.201e−3	0.010014	0.014909	0.019827	0.024754
GaSb	Ga	2.063e−3	4.483e−3	8.197e−3	0.015973	0.02384	0.031731	0.039631
	Sb	1.531e−3	3.734e−3	7.010e−3	0.013776	0.020595	0.027427	0.034266
InN	In	1.160e−3	1.905e−3	3.338e−3	6.422e−3	9.560e−3	0.012713	0.015872
	N	2.631e−3	3.177e−3	4.214e−3	6.780e−3	9.622e−3	0.012562	0.015544
InP	In	1.654e−3	3.637e−3	6.785e−3	0.013312	0.019895	0.026493	0.033096
	P	2.407e−3	3.831e−3	6.223e−3	0.011555	0.017069	0.022634	0.028219
InAs	In	1.785e−3	4.616e−3	8.742e−3	0.017226	0.025765	0.03432	0.04288
	As	1.847e−3	4.114e−3	7.520e−3	0.01465	0.021864	0.029099	0.036344
InSb	In	1.958e−3	6.102e−3	0.011711	0.023163	0.034671	0.046194	0.057723
	Sb	1.724e−3	5.274e−3	0.010085	0.019926	0.029821	0.039728	0.049642
MgS	Mg	2.525e−3	0.011639	0.021684	0.042386	0.063289	0.084248	0.10523
	S	2.033e−3	0.015568	0.030296	0.060115	0.090034	0.11998	0.149938
MgSe	Mg	2.817e−3	8.918e−3	0.016065	0.031072	0.046298	0.061585	0.076897
	Se	1.290e−3	0.012281	0.024229	0.04828	0.07237	0.096469	0.120573
MgTe	Mg	4.177e−3	7.855e−3	0.013642	0.026102	0.038812	0.051589	0.064394
	Te	1.998e−3	5.696e−3	0.010938	0.021641	0.032395	0.043163	0.053936
ZnS	Zn	2.229e−3	3.942e−3	7.046e−3	0.013641	0.020335	0.027053	0.033781
	S	2.425e−3	3.504e−3	5.565e−3	0.010258	0.015132	0.020054	0.024997
ZnSe	Zn	2.397e−3	4.890e−3	8.938e−3	0.017424	0.026008	0.034617	0.043237
	Se	1.808e−3	3.617e−3	6.547e−3	0.012721	0.018976	0.025252	0.031536
ZnTe	Zn	2.559e−3	5.895e−3	0.01094	0.021428	0.032014	0.042626	0.053247
	Te	1.615e−3	4.194e−3	7.941e−3	0.015648	0.023407	0.031178	0.038955
CdS	Cd	2.110e−3	5.610e−3	0.010709	0.021152	0.031653	0.042169	0.052691
	S	2.789e−3	5.063e−3	8.628e−3	0.016373	0.024302	0.032282	0.040282
CdSe	Cd	2.258e−3	6.928e−3	0.013343	0.02642	0.039555	0.052706	0.065862
	Se	2.090e−3	5.380e−3	0.010064	0.019753	0.029524	0.039316	0.049116
CdTe	Cd	1.652e−3	3.516e−3	6.516e−3	0.012766	0.019075	0.025398	0.031727
	Te	1.602e−3	3.631e−3	6.804e−3	0.013374	0.019995	0.026629	0.033268
C	C	1.611e−3	1.626e−3	1.690e−3	1.986e−3	2.436e−3	2.962e−3	3.529e−3
Si	Si	2.471e−3	3.196e−3	4.865e−3	8.772e−3	0.01287	0.017022	0.021198
Ge	Ge	1.718e−3	3.191e−3	5.665e−3	0.01093	0.01628	0.021653	0.027035

static correlation function. Inserting equation (41) into equation (40) yields a relationship between the $\langle u^2(\nu; T)\rangle$ and the parameters A, B and σ:

$$\langle u^2(\nu; T)\rangle = \frac{\hbar}{2M_\nu}\frac{\coth\{\hbar[A\exp(-T^2/\sigma^2)+B]/2k_{\rm B}T\}}{[A\exp(-T^2/\sigma^2)+B]}. \quad (42)$$

Using equation (42) and optimizing the parameters A, B and σ, the curve shown as a line in Fig. 13 can be generated. Additionally Fig. 13 depicts the temperature dependence of the static correlation function as calculated from equation (35). Fig. 13 shows a very good agreement of the fit with the calculated values.

In Tables 4 and 5 fit parameters for the temperature dependence of the characteristic frequency of II–VI, III–V and group IV semiconductors are listed. As mentioned in §3.1.1, the bond length is underestimated in the LDA and overestimated in the GGA. This should also be the case for the Debye–Waller factors (Vila *et al.*, 2007). However, we compared our computed phonon dispersion relations with measured ones for GaP (Kunc *et al.*, 1975), GaAs (Strauch & Dorner, 1990), GaSb (Farr *et al.*, 1975), InP (Borcherds *et al.*, 1975), InSb (Banerjee & Varshni, 1969), ZnS (Vagelatos *et al.*, 1974), ZnSe (Hennion *et al.*, 1971), ZnTe (Vagelatos *et al.*, 1974), CdTe (Rowe *et al.*, 1974), diamond (Warren *et al.*, 1967), Si (Nilsson & Nelin, 1972) and Ge (Nilsson & Nelin, 1971). For the III–V and group IV materials our LDA results are in much better agreement than the GGA calculations, but for the II–VI compounds the opposite is true. Since the Debye–Waller factors were derived from the computed phonon frequency this should also hold for the Debye–Waller factors. Therefore

Table 6 lists mean-square displacements computed within the LDA for the III–V and group IV materials and within the GGA for the II–VI materials for selected temperatures.

A measurement of the Debye–Waller factors for GaAs by Stahn *et al.* (1998) at 287 K supports this finding. They found static correlation functions $\langle u^2(\mathrm{Ga})\rangle = 0.00844\ \text{Å}^2$ and $\langle u^2(\mathrm{As})\rangle = 0.00716\ \text{Å}^2$. Our computation within the LDA yielded $\langle u^2(\mathrm{Ga})\rangle = 0.00845\ \text{Å}^2$ and $\langle u^2(\mathrm{As})\rangle = 0.00726\ \text{Å}^2$, and within the GGA $\langle u^2(\mathrm{Ga})\rangle = 0.00927\ \text{Å}^2$ and $\langle u^2(\mathrm{As})\rangle = 0.00779\ \text{Å}^2$ for the temperature at which the measurement of Stahn *et al.* (1998) was performed. The agreement is excellent for the LDA, but deviations are present for the GGA, which is in agreement with the above statement. In Table 7 computed Debye–Waller factors are compared with further measurements and the calculation by Reid (1983).

Using the fit parameters of Gao & Peng (1999), one can deduce $\langle u^2(\mathrm{Ga})\rangle = 0.00784\ \text{Å}^2$ and $\langle u^2(\mathrm{As})\rangle = 0.00844\ \text{Å}^2$. Comparing these values with the experimental values suggests an interchange of the Debye–Waller factors of Ga and As. However, even in the original paper by Reid (1983), to which Gao and Peng fitted their temperature dependence, the Debye–Waller factor of Ga was given to be smaller than that of As.

Table 7
Comparison of mean-square displacements (Å^2).

The computed mean-square displacements are compared with experimental values and the values of the shell model of Reid & Pirie (1980) for group IV semiconductors and the valence-shell model of Reid (1983) for II–VI semiconductors. Experimental Debye–Waller factors were taken from Yoshiasa *et al.* (1997) and McIntyre *et al.* (1980) except for the measurements for Si and diamond, which were taken from Midgley *et al.* (1998). Values are compared at the temperature at which measurements were performed, which was 295 K apart from Si and diamond (100 K).

		Mean-square displacement		
Material	Element	Computed	Experimental	Reid
Si	Si	0.0032	0.0032	0.0032
C	C	0.0016	0.0017	0.0016
Ge	Ge	0.0082	0.0052	0.0076
ZnS	Zn	0.0102	0.0111	0.0108
	S	0.0078	0.0090	0.0093
ZnSe	Zn	0.0130	0.0129	0.0125
	Se	0.0095	0.0090	0.0084
ZnTe	Zn	0.0160	0.0164	0.0169
	Te	0.0120	0.0096	0.0121
CdS	Cd	0.0157	0.0176	
	S	0.0123	0.0144	
CdSe	Cd	0.0200	0.0200	
	Se	0.0150	0.0160	

5. Summary

In summary, we have computed phonon dispersion curves for nonpolar group IV and polar II–VI and III–V semiconductors within a density functional theory approach. To get the LO–TO splitting for polar semiconductors, we also computed Born effective charges and dielectric constants within a density functional perturbation theory approach. The calculated phonon dispersion relations were in good agreement with measured phonon frequencies taken from the literature. The Debye–Waller factors were then derived from generalized phonon densities of states. Subsequently an accurate fitting function was derived for the temperature dependence of the Debye–Waller factor using a temperature-dependent characteristic frequency.

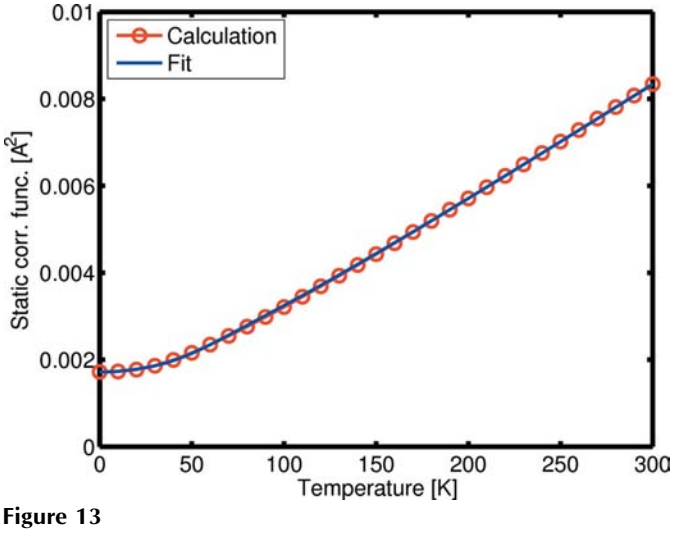

Figure 13
Fit of the static correlation function of Ge using the temperature dependence of the characteristic frequency shown in Fig. 12.

This work was supported by the Deutsche Forschungsgemeinschaft under contract No. RO2057/4-1 and by the FWO-Vlaanderen under project G.0425.05. We have also benefitted from computer time on the CalcUA supercomputer of the University of Antwerp. The authors also acknowledge financial support from the European Union under the Framework 6 program under a contract for an Integrated Infrastructure Initiative (reference 026019 ESTEEM).

References

Banerjee, R. & Varshni, Y. P. (1969). *Can. J. Phys.* **47**, 451–462.
Blaha, P., Schwarz, K., Madsen, G. K. H., Kvasnicka, D. & Luitz, J. (2001). *Wien2k, An Augmented Plane Wave + Local Orbitals Program for calculating crystal properties*, K. Schwarz, Technische Universität Wien, Austria. ISBN 3-9501031-1-2.
Borcherds, P. H., Alfrey, G. F., Woods, A. D. B. & Saunderson, D. H. (1975). *J. Phys. C Solid State Phys.* **8**, 2022–2030.
Ceperley, D. M. & Alder, B. J. (1980). *Phys. Rev. Lett.* **45**, 566–569.
Cochran, W. & Cowley, R. A. (1962). *J. Phys. Chem. Solids*, **23**, 447–450.
Doyle, P. A. & Turner, P. S. (1968). *Acta Cryst.* A**24**, 390–397.
Einstein, A. (1911). *Ann. Phys.* **35**, 679–694.
Farr, M. K., Traylor, J. G. & Sinha, S. K. (1975). *Phys. Rev. B*, **11**, 1587–1594.
Gao, H. X. & Peng, L.-M. (1999). *Acta Cryst.* A**55**, 926–932.
Gironcoli, S. de, Baroni, S. & Resta, R. (1989). *Phys. Rev. Lett.* **62**, 2853–2856.
Gonze, X., Beuken, J.-M., Caracas, R., Detraux, F., Fuchs, M., Rignanese, G.-M., Sindic, L., Verstraete, M., Zerah, G., Jollet, F., Torrent, M., Roy, A., Mikami, M., Ghosez, Ph., Raty, J.-Y. & Allan, D. C. (2002). *Comput. Mater. Sci.* **25**, 478–492.
Gonze, X. & Lee, C. (1997). *Phys. Rev. B*, **55**, 10355–10368.

Hennion, B., Moussa, F., Pepy, G. & Kunc, K. (1971). *Phys. Lett. A*, **36**, 376–378.
Kittel, C. (1988). *Einführung in die Festkörperphysik, Anhang A*. Munich: R. Oldenbourg Verlag.
Kunc, K., Balkanski, M. & Nusimovici, M. A. (1975). *Phys. Rev. B*, **12**, 4346–4355.
Lee, C. & Gonze, X. (1995). *Phys. Rev. B*, **51**, 8610–8613.
Loane, R. F., Xu, P. & Silcox, J. (1991). *Acta Cryst.* A**47**, 267–278.
Maradudin, A. A. (1971). *Solid State Physics*. New York: Academic Press.
McIntyre, G. J., Moss, G. & Barnea, Z. (1980). *Acta Cryst.* A**36**, 482–490.
Midgley, P. A., Sleight, M. E., Saunders, M. & Vincent, R. (1998). *Ultramicroscopy*, **75**, 61–67.
Nilsson, G. & Nelin, G. (1971). *Phys. Rev. B*, **3**, 364–369.
Nilsson, G. & Nelin, G. (1972). *Phys. Rev. B*, **6**, 3777–3786.
Parlinski, K., Li, Z. Q. & Kawazoe, Y. (1997). *Phys. Rev. Lett.* **78**, 4063–4066.
Perdew, J. P., Burke, K. & Ernzerhof, M. (1996). *Phys. Rev. Lett.* **77**, 3865–3868.
Perdew, J. P. & Wang, Y. (1992). *Phys. Rev. B*, **45**, 13244–13249.
Reid, J. S. (1983). *Acta Cryst.* A**39**, 1–13.
Reid, J. S. & Pirie, J. D. (1980). *Acta Cryst.* A**36**, 957–965.
Rosenauer, A., Schowalter, M., Glas, F. & Lamoen, D. (2005). *Phys. Rev. B*, **72**, 085326.
Rother, A. & Lichte, H. (2007). *Microsc. Microanal.* **13**, 26.
Rowe, J. M., Nicklow, R. M., Price, D. L. & Zanio, K. (1974). *Phys. Rev. B*, **10**, 671–675.
Sears, V. F. & Shelley, S. A. (1991). *Acta Cryst.* A**47**, 441–446.
Stahn, J., Möhle, M. & Pietsch, U. (1998). *Acta Cryst.* B**54**, 231–239.
Strauch, D. & Dorner, B. (1990). *J. Phys. Condens. Matter*, **2**, 1457–1474.
Troullier, N. & Martins, J. L. (1991). *Phys. Rev. B*, **43**, 1993–2006.
Vagelatos, N., Wehe, D. & King, J. S. (1974). *J. Chem. Phys.* **60**, 3613–3618.
Vetelino, J. F., Gaur, S. P. & Mitra, S. S. (1972). *Phys. Rev. B*, **5**, 2360–2366.
Vila, F. D., Rehr, J. J., Rossner, H. H. & Krappe, J. (2007). *Phys. Rev. B*, **76**, 014301.
Warren, J. L., Yarnell, J. L., Dolling, G. & Cowley, R. A. (1967). *Phys. Rev.* **158**, 805–808.
Weickenmeier, A. & Kohl, H. (1991). *Acta Cryst.* A**47**, 590–597.
Yoshiasa, A., Koto, K., Maeda, H. & Ishi, T. (1997). *Jpn. J. Appl. Phys.* **36**, 781–784.
Zuo, J. M., Blaha, P. & Schwarz, K. (1997). *J. Phys. Condens. Matter*, **9**, 7541–7561.